



HAL
open science

Modulational instability in isolated and driven Fermi–Pasta–Ulam lattices

Thierry Dauxois, R Khomeriki, S Ruffo

► **To cite this version:**

Thierry Dauxois, R Khomeriki, S Ruffo. Modulational instability in isolated and driven Fermi–Pasta–Ulam lattices. *The European Physical Journal. Special Topics*, 2007, 147, pp.3. 10.1140/epjst/e2007-00200-2 . hal-01139473

HAL Id: hal-01139473

<https://hal.science/hal-01139473>

Submitted on 5 Apr 2015

HAL is a multi-disciplinary open access archive for the deposit and dissemination of scientific research documents, whether they are published or not. The documents may come from teaching and research institutions in France or abroad, or from public or private research centers.

L'archive ouverte pluridisciplinaire **HAL**, est destinée au dépôt et à la diffusion de documents scientifiques de niveau recherche, publiés ou non, émanant des établissements d'enseignement et de recherche français ou étrangers, des laboratoires publics ou privés.

Modulational instability in isolated and driven Fermi-Pasta-Ulam lattices

Thierry Dauxois^{1,a}, Ramaz Khomeriki^{2,3,b}, and Stefano Ruffo^{2,c}

¹ Laboratoire de Physique, UMR-CNRS 5672, ENS Lyon, 46 Allée d'Italie, 69364 Lyon cédex 07, France

² Dipartimento di Energetica, “S. Stecco” and CSDC, Università di Firenze, and INFN, via S. Marta, 3, 50139 Firenze, Italy

³ Department of Exact and Natural Sciences, Tbilisi State University, 3 Chavchavadze avenue, Tbilisi 0128, Georgia

Abstract. We present a detailed analysis of the modulational instability of the zone-boundary mode for one and higher-dimensional Fermi-Pasta-Ulam (FPU) lattices. The growth of the instability is followed by a process of relaxation to equipartition, which we have called the *Anti-FPU problem* because the energy is initially fed into the highest frequency part of the spectrum, while in the original FPU problem low frequency excitations of the lattice were considered. This relaxation process leads to the formation of *chaotic breathers* in both one and two space dimensions. The system then relaxes to energy equipartition, on time scales that increase as the energy density is decreased. We supplement this study by considering the nonconservative case, where the FPU lattice is homogeneously driven at high frequencies. Standing and travelling nonlinear waves and solitonic patterns are detected in this case. Finally we investigate the dynamics of the FPU chain when one end is driven at a frequency located above the zone boundary. We show that this excitation stimulates nonlinear bandgap transmission effects.

1 Introduction

In 1955, reporting about one of the first numerical simulations, Fermi, Pasta and Ulam (FPU) [1] remarked that it was ... *very hard to observe the rate of “thermalization” or mixing* ... in a nonlinear one-dimensional lattice in which the energy was initially fed into the lowest frequency mode. Even if the understanding of this problem has advanced significantly afterwards [2, 3], several issues are still far from being clarified. In most cases, the evolution towards energy *equipartition* among linear modes has been checked considering an initial condition where all the energy of the system was concentrated in a small packet of modes centered around some low frequency.

Beginning with the pioneering paper of Zabusky and Deem [4], the opposite case in which the energy is put into a high frequency mode has been also analyzed. In this early paper, the zone-boundary mode was excited with an added spatial modulation for the one-dimensional α -FPU model (quadratic nonlinearity in the equations of motion). Here, we will study the time-evolution of this mode without any spatial modulation for the β -FPU model (cubic nonlinearity in the equations of motion) and some higher-order nonlinearities. Moreover, we will extend the

^a e-mail: Thierry.Dauxois@ens-lyon.fr

^b e-mail: khomeriki@hotmail.com

^c e-mail: Stefano.Ruffo@unifi.it

study to higher dimensional lattices. Since the energy is fed into the opposite side of the linear spectrum, we call this problem the *Anti-FPU problem*.

In a paper by Bundinsky and Bountis [5], the zone-boundary mode solution of the one-dimensional FPU lattice was found to be unstable above an energy threshold E_c which scales like $1/N$, where N is the number of oscillators. This result was later and independently confirmed by Flach [6] and Poggi et al [7], who also obtained the correct factor in the large N -limit. These results were obtained by a direct linear stability analysis around the periodic orbit corresponding to the zone-boundary mode. Similar methods have been recently applied to other modes and other FPU-like potentials by Chechin et al [8,9] and Rink [10].

A formula for E_c , valid for all N , has been obtained in Refs. [13,12,11,14] in the rotating wave approximation, and will be also discussed in this paper. Associated with this instability is the calculation of the growth rates of mode amplitudes. The appropriate approach for Klein-Gordon lattices was first introduced by Kivshar and Peyrard [15], following an analogy with the Benjamin-Feir instability in fluid mechanics [16].

Previously, a completely different approach to describe this instability was introduced by Zakharov and Shabat [17], studying the associated Nonlinear Schrödinger equation in the continuum limit. A value for the energy threshold was obtained in Ref. [18] in the continuum limit. The full derivation starting from the FPU equation of motions was then independently obtained by Berman and Kolovskii [19] in the so-called “narrow-packet” approximation.

Only very recently the study of what happens after the modulational instability develops has been performed for Klein-Gordon [20] and FPU-lattices[21,13]. From these analyses it turned out that these high-frequency initial conditions lead to a completely new dynamical behavior in the transient time preceding the final energy equipartition. In particular, the main discovery has been the presence on the lattice of sharp localized modes [21,20]. These latter papers were the first to make the connection between energy relaxation and intrinsic localized modes [22], or breathers [23]. Later on, a careful numerical and theoretical study of the dynamics of a β -FPU model was performed [24]. It has been shown that moving breathers play a relevant role in the transient dynamics and that, contrary to exact breathers, which are periodic solutions, these have a chaotic evolution. This is why they have been called *chaotic breathers*. Following these studies, Lepri and Kosevich [25] and Lichtenberg and coworkers [26,27] have further characterized the scaling laws of relaxation times using continuum limit equations.

Zabusky et al. have recently simulated numerically the behavior of the one-dimensional, periodic α -FPU model with optical and acoustic initial excitations of small-but finite and large amplitudes. Using beautiful color representations [28] of the numerical results, they find nearly recurrent solutions, where the optical result is due to the appearance of localized breather-like packets. For large amplitudes, they obtained also chaotic behaviors for the alpha lattice.

Using a theory (originally developed [29,30] for the discrete nonlinear Schrödinger equation) where standard Gibbsian equilibrium statistical mechanics was considered to predict macroscopic average values for a thermalized state in the thermodynamic limit, Johansson has recently analyzed [31] certain aspects of a mixed Klein-Gordon/FPU chain. In particular, he shows that the available phase space is divided into two separated parts with qualitatively different properties in thermal equilibrium: one part corresponding to a normal thermalized state with exponentially small probabilities for large-amplitude excitations, and another part typically associated with the formation of high-amplitude localized excitations, interacting with an infinite-temperature phonon bath. Observing the β -FPU chains in the thermalized state, Gershgorin et al showed [32] via numerical simulation that discrete breathers actually persist and have a turbulent-like behavior. They describe the dynamical scenario as spatially highly localized discrete breathers riding chaotically on spatially extended, renormalized waves.

Recently Flach et al [33] have focused on the main FPU observation that the initially excited normal mode shares its energy for long times only with a few other modes from a frequency neighbourhood in modal space. They have identified this long lasting regime as a dynamical localization effect and applied the methods developed for discrete breathers in FPU chains to the dynamics of normal modes. The result is that time-periodic and modal-space-localized orbits, (they call q-breathers) persist in the FPU model. The dynamics generated by one initially excited mode evolves close to the related q-breathers for very long times. Thus many features

of the short- and medium-time evolution of natural packets are encoded in the profile of these objects.

Let us briefly comment about the chaoticity of these spontaneously created breathers. Tailleur and Kurchan have recently implemented [34] an efficient method that allows one to select trajectories with unusual chaoticity, with Lyapunov weighted dynamics (LWD) (a method originally proposed in the context of chemical reactions [35]). As an example of application, they study the Fermi-Pasta-Ulam nonlinear chain starting from a microcanonical equilibrium configuration. They show that the algorithm rapidly singles out the chaotic-breathers when searching for trajectories with high level of chaoticity (typically they study cases where the Lyapunov is three times the one of a typical equilibrium trajectory), thus confirming that the large Lyapunov configurations are dominated by chaotic breathers.

Most of the previous studies are for one-dimensional lattices. We have recently derived modulational instability thresholds also for higher dimensional lattices [36] and we have presented a study of chaotic breathers formation in two-dimensional FPU lattices. However, the study is extremely preliminary and further analyses are needed. In particular, the full process of relaxation to energy equipartition and the associated time scales have not been carefully studied in two-dimensional FPU lattices. Pioneering results on the relaxation process in a two-dimensional triangular FPU lattice from low frequency initial states seem to indicate a faster evolution to equipartition [61]. Benettin has discovered that for large values of the energy per site the time scale for equipartition can be quite short, even in the thermodynamic limit of the lattice size, and that this time scale increases as only one-over the energy per site. If one lowers the energy per site below a critical threshold, however, the time scale for equipartition on finite lattices grows much more rapidly. But the critical threshold value of energy per site appears to vanish as the lattice size goes to infinity. A similar analysis for high frequencies remains to be performed.

Further, having already studied the process of formation of stable localized structures arising from modulational instability in the conservative case [24], we are strongly motivated to see how the presence of forcing and damping affects this process. To remain close to the Hamiltonian case, we restrict ourselves to the case of small damping. Various types of forcing are in principle possible, depending on the physical situation under study. However, a general requirement for localization is to excite band-edge modes. For Klein-Gordon lattices this is naturally realized using a spatially uniform driving field, which has been shown to induce interesting pattern formation phenomena [37]. On the other hand, this forcing would not be effective for FPU lattices, because, due to the symmetry of the Hamiltonian, the zero mode is decoupled. Alternatively, since spatial localization appears from the instability of band-edge modes, we choose in the context of Anti FPU scenario to drive the system near the zone boundary wavelength. As it will be shown below stationary localized patterns (either moving or static) appear under such a homogeneous driving and damping.

Finally, we consider driving the system by one end, again with frequencies above the zone boundary. By this we stimulate the appearance of a “supratransmission” scenario [38] in FPU, i.e. the chain becomes conductive only for driving amplitudes above a threshold [39]. This phenomenon is explained in terms of nonlinear response manifolds in Ref. [40].

We have organized the paper in the following way. In Section 2, the modulational instability of zone-boundary modes on the lattice is discussed, beginning with the one-dimensional case, followed by the two-dimensional and higher dimensional cases and finishing with the continuum nonlinear Schrödinger approach. In this Section, we also describe the mechanism of creation of chaotic breathers in one and two dimensions. Section 3 deals with the driven-damped Anti-FPU scenario (homogeneous and point-like driving). Some final remarks and conclusions are reported in Section 4.

2 Modulational Instability

2.1 The one-dimensional case

We will discuss in this section modulational instability for the one-dimensional FPU lattice, where the linear coupling is corrected by a $(2\ell + 1)$ th order nonlinearity, with ℓ a positive

integer. Denoting by $u_n(t)$ the relative displacement of the n -th particle from its equilibrium position, the equations of motion are

$$\ddot{u}_n = u_{n+1} + u_{n-1} - 2u_n + (u_{n+1} - u_n)^{2\ell+1} - (u_n - u_{n-1})^{2\ell+1}. \quad (1)$$

We adopt a lattice of N particles and we choose periodic boundary conditions. For the sake of simplicity, we first report on the analysis for $\ell = 1$ (i.e. for the β -FPU model) and then we generalize the results to any ℓ -value.

Due to periodic boundary conditions, the normal modes associated to the linear part of Eq. (1) are plane waves of the form

$$u_n(t) = \frac{a}{2} \left(e^{i\theta_n(t)} + e^{-i\theta_n(t)} \right) \quad (2)$$

where $\theta_n(t) = qn - \omega t$ and $q = 2\pi k/N$ ($k = -N/2, \dots, N/2$). The dispersion relation of nonlinear phonons in the rotating wave approximation [13] is $\omega^2(q) = 4(1 + \alpha) \sin^2(q/2)$, where $\alpha = 3a^2 \sin^2(q/2)$ takes into account the nonlinearity. Modulational instability of such a plane wave is investigated by studying the linearized equation associated with the envelope of the carrier wave (2). Therefore, one introduces infinitesimal perturbations in the amplitude and phase and looks for solutions of the form

$$\begin{aligned} u_n(t) &= \frac{a}{2} [1 + b_n(t)] e^{i[\theta_n(t) + \psi_n(t)]} + \frac{a}{2} [1 + b_n(t)] e^{-i[\theta_n(t) + \psi_n(t)]} \\ &= a[1 + b_n(t)] \cos[qn - \omega t + \psi_n(t)], \end{aligned} \quad (3)$$

where b_n and ψ_n are reals and assumed to be small in comparison with the parameters of the carrier wave. Substituting Eq. (3) into the equations of motion and keeping the second derivative, we obtain for the real and imaginary part of the secular term $e^{i(qn - \omega t)}$ the following equations

$$\begin{aligned} -\omega^2 b_n + 2\omega \dot{\psi}_n + \ddot{b}_n &= (1 + 2\alpha) [\cos q (b_{n+1} + b_{n-1}) - 2b_n] \\ &\quad - \alpha (b_{n+1} + b_{n-1} - 2b_n \cos q) - (1 + 2\alpha) \sin q (\psi_{n+1} - \psi_{n-1}) \quad (4) \\ -\omega^2 \psi_n - 2\omega \dot{b}_n + \ddot{\psi}_n &= (1 + 2\alpha) [\cos q (\psi_{n+1} + \psi_{n-1}) - 2\psi_n] \\ &\quad + (1 + 2\alpha) \sin q (b_{n+1} - b_{n-1}) + \alpha (\psi_{n+1} + \psi_{n-1} - 2\psi_n \cos q). \quad (5) \end{aligned}$$

Further assuming $b_n = b_0 e^{i(Qn - \Omega t)} + \text{c.c.}$ and $\psi_n = \psi_0 e^{i(Qn - \Omega t)} + \text{c.c.}$ we obtain the following equations for the secular term $e^{i(Qn - \Omega t)}$

$$\begin{aligned} b_0 \left[\Omega^2 + \omega^2 + 2(1 + 2\alpha)(\cos q \cos Q - 1) - 2\alpha(\cos Q - \cos q) \right] \\ - 2i\psi_0 [\omega\Omega + (1 + 2\alpha) \sin q \sin Q] = 0 \quad (6) \end{aligned}$$

$$\begin{aligned} \psi_0 \left[\Omega^2 + \omega^2 + 2(1 + 2\alpha)(\cos q \cos Q - 1) + 2\alpha(\cos Q - \cos q) \right] \\ + 2ib_0 [\omega\Omega + (1 + 2\alpha) \sin q \sin Q] = 0. \quad (7) \end{aligned}$$

In the case of Klein-Gordon type equations [15, 20], one neglects the second order derivatives in Eqs. (4)-(5). This can be justified by the existence of a gap in the dispersion relation for $q = 0$, which allows to neglect Ω^2 with respect to ω^2 . In the FPU case, this approximation is worse, especially for long wavelengths, because there is no gap.

Non trivial solutions for Eqs. (6)-(7) can be found only if the Cramer's determinant vanishes, i.e. if the following equation is fulfilled:

$$\begin{aligned} \left[(\Omega + \omega)^2 - 4(1 + 2\alpha) \sin^2 \left(\frac{q + Q}{2} \right) \right] \left[(\Omega - \omega)^2 - 4(1 + 2\alpha) \sin^2 \left(\frac{q - Q}{2} \right) \right] \\ = 4\alpha^2 (\cos Q - \cos q)^2. \quad (8) \end{aligned}$$

This equation admits four different solutions when the wavevectors q of the unperturbed wave and Q of the perturbation are fixed. If one of the solutions is complex, an instability of one of the modes ($q \pm Q$) is present, with a growth rate equal to the imaginary part of the solution. Using this method, one can derive the instability threshold amplitude for any wavenumber. A trivial example is the case of $q = 0$, for which we obtain $\Omega = \pm \sin(Q/2)$, which proves that the zero mode solution is stable. This mode is present due to the invariance of the equations of motion (1) with respect to the translation $u_n \rightarrow u_n + \text{const}$ and, as expected, is completely decoupled from the others.

A first interesting case is $q = \pi$. One can easily see that Eq. (8) admits two real and two complex conjugate imaginary solutions if and only if

$$\cos^2 \frac{Q}{2} > \frac{1 + \alpha}{1 + 3\alpha}. \quad (9)$$

This formula was first obtained by Sandusky and Page (Eq. (22) in Ref. [13]) using the rotating wave approximation. The first mode to become unstable when increasing the amplitude a corresponds to the wavenumber $Q = 2\pi/N$. Therefore, the critical amplitude a_c above which the $q = \pi$ -mode loses stability is

$$a_c = \left(\frac{\sin^2(\pi/N)}{3[3\cos^2(\pi/N) - 1]} \right)^{1/2}. \quad (10)$$

This formula is valid for all even values of N and its large N -limit is

$$a_c = \frac{\pi}{\sqrt{6}N} + O\left(\frac{1}{N^3}\right). \quad (11)$$

In Fig. 1, we show its extremely good agreement with the critical amplitude determined from numerical simulations. It is interesting to emphasize that the analytical formula (10) diverges for $N = 2$, predicting that the π -mode is stable for all amplitudes in this smallest lattice. This is in agreement with the Mathieu equation analysis (see Ref. [7] p. 265).

It is also interesting to express this result in terms of the total energy to compare with what has been obtained using other methods [17, 5, 19, 6, 7]. Since for the π -mode the energy is given by $E = N(2a^2 + 4a^4)$, we obtain the critical energy

$$E_c = \frac{2N}{9} \sin^2\left(\frac{\pi}{N}\right) \frac{7\cos^2(\pi/N) - 1}{[3\cos^2(\pi/N) - 1]^2}. \quad (12)$$

For large N , we get

$$E_c = \frac{\pi^2}{3N} + O\left(\frac{1}{N^3}\right). \quad (13)$$

This asymptotic behavior is the same as the one obtained using the narrow packet approximation in the context of the nonlinear Schrödinger equation by Berman and Kolovskii (Eq. (4.1) in Ref. [19]). The correct scaling behavior with N of the critical energy has been also obtained by Bundinsky and Bountis (Eq. (2.22) in Ref. [5]) by a direct linear stability analysis of the π -mode. The correct formula, using this latter method, has been independently obtained by Flach (Eq. (3.20)) in Ref. [6] and Poggi and Ruffo (p. 267 of Ref. [7]). Recently, the N^{-1} -scaling of formula (13) has been confirmed using a different numerical method and, interestingly, it holds also for the $2\pi/3$ and $\pi/2$ modes [41].

This critical energy is also very close to the Chirikov “stochasticity threshold” energy obtained by the resonance overlap criterion for the zone boundary mode [42]. The stochasticity threshold phenomenon has been thoroughly studied for long wavelength initial conditions, and it has been clarified that it corresponds to a change in the scaling law of the largest Lyapunov exponent [43]. We will show in Section 3 that above the modulational instability critical energy for the π -mode one reaches asymptotically a chaotic state with a positive Lyapunov exponent, consistently with Chirikov’s result.

The above results can be generalized to nonlinearities of $2\ell + 1$ order in the equations of motion (1). We limit the analysis to the π -mode, for which the instability condition (9) takes the form

$$\cos^2 \frac{Q}{2} > \frac{1 + \alpha}{1 + (2\ell + 1)\alpha}, \quad (14)$$

where

$$\alpha = \frac{(2\ell + 1)!}{\ell!(\ell + 1)!} a^{2\ell}. \quad (15)$$

Hence the critical amplitude above which the π -mode is unstable is

$$a_c = \left[\frac{\ell!(\ell + 1)! \sin^2(\pi/N)}{(2\ell + 1)! [(2\ell + 1) \cos^2(\pi/N) - 1]} \right]^{1/2}, \quad (16)$$

leading to the large N scaling

$$a_c \sim N^{-1/\ell} \quad (17)$$

$$E_c \sim N^{1-2/\ell}. \quad (18)$$

This scaling also corresponds to the one found in Ref. [44] when discussing tangent bifurcations of band edge plane waves in relation with energy thresholds for discrete breathers. Their “de-tuning exponent” z has a direct connection with the nonlinearity exponent $\ell = z/2$. We will see in Section 2.2 that this analogy extends also to higher dimensions.

For fixed N , a_c is an increasing function of the power of the coupling potential with the asymptotic limit $\lim_{\ell \rightarrow \infty} a_c = 0.5$. Therefore, in the hard potential limit the critical energy for the π -mode increases proportionally to N . The fact that we find a higher energy region where the system is chaotic is not in contradiction with the integrability of the one-dimensional system of hard rods[45], because in the present case we have also a harmonic contribution at small distances.

For the FPU- α model (quadratic nonlinearity in the equations of motion), the π -mode is also an exact solution which becomes unstable at some critical amplitude which, contrary to the case of the FPU- β model, is N -independent[13,8]; which means that the critical energy is proportional to N and then that π -mode can be stable in some low energy density limit also in the thermodynamic limit.

It has also been realized [7,47,46,8,48,10] that group of modes form sets which are invariant under the dynamics. The stability analysis [46,9] of pair of modes has shown a complex dependence on their relative amplitudes. The existence of such invariant manifolds has also allowed to construct Birkhoff-Gustavson normal forms for the FPU model, paving the way to KAM theory [49].

2.2 Higher dimensions

In this Section, we will first discuss modulational instability of the two-dimensional FPU model. The method presented in Section 2.1 can be easily extended and the global physical scenario is preserved. However, the scaling with N of the critical amplitude changes in such a way to make critical energy constant, in agreement with the analysis of Ref. [44].

The masses lie on a two-dimensional square lattice with unitary spacing in the (x, y) plane. We consider a small relative displacement $u_{n,m}$ ($n, m \in [1, N]$) in the vertical direction z . Already with an harmonic potential, if the spring length at equilibrium is not unitary, the series expansion in $u_{n,m}$ of the potential contains all even powers. We retain only the first two terms of this series expansion. After an appropriate rescaling of time and displacements to eliminate mass and spring constant values, one gets the following adimensional equations of motions

$$\begin{aligned} \ddot{u}_{n,m} = & u_{n+1,m} + u_{n-1,m} + u_{n,m+1} + u_{n,m-1} - 4u_{n,m} \\ & + (u_{n+1,m} - u_{n,m})^3 + (u_{n-1,m} - u_{n,m})^3 + (u_{n,m+1} - u_{n,m})^3 + (u_{n,m-1} - u_{n,m})^3 \end{aligned} \quad (19)$$

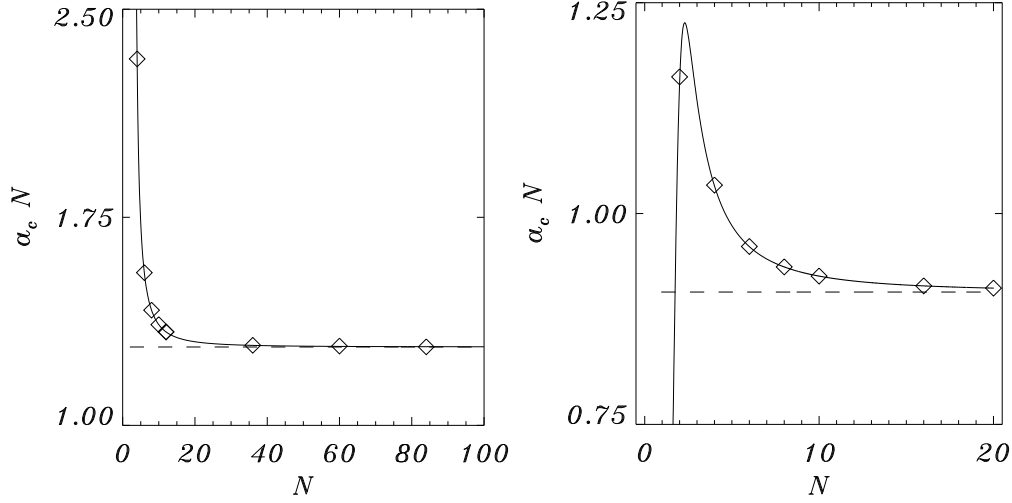


Fig. 1. Left panel: Modulational instability threshold amplitude for the π -mode versus the number of particles in the one-dimensional FPU lattice. The solid line corresponds to the analytical formula (10), the dashed line to its large N -estimate (11) and the diamonds are obtained from numerical simulations. Right panel: Modulation instability threshold for the (π, π) mode versus number of oscillators in two dimensional array. Solid line is derived from the exact analytical consideration (30), dashed line describes the estimate from NLS equation in large N limit (43) and diamonds are result of numerical simulations.

Considering periodic boundary conditions, plane waves solutions have the form

$$u_{n,m} = a \cos(q_x n + q_y m - \omega t). \quad (20)$$

In the rotating wave approximation[13], one immediately obtains the dispersion relation

$$\omega^2 = 4 \sin^2 \frac{q_x}{2} + 4 \sin^2 \frac{q_y}{2} + 12a^2 \left[\sin^4 \frac{q_x}{2} + \sin^4 \frac{q_y}{2} \right], \quad (21)$$

which becomes exact for the zone-boundary mode $(q_x, q_y) = (\pi, \pi)$,

$$\omega_{\pi,\pi}^2 = 8(1 + 3a^2). \quad (22)$$

To study the stability of the zone-boundary mode, we adopt a slightly different approach. Namely, we consider the perturbed relative displacement field of the form

$$u_{n,m} = \left(\frac{a}{2} + b_{n,m} \right) e^{i(\pi n + \pi m - \omega_{\pi,\pi} t)} + c.c., \quad (23)$$

where $b_{n,m}$ is complex. This approach turns out to be equivalent to the one of Section 2.1 in the linear limit.

Substituting this perturbed displacement field in Eqs. (19), we obtain

$$[1 + 2\alpha] [b_{n+1,m} + b_{n-1,m} + b_{n,m+1} + b_{n,m-1} + 4b_{n,m}] - \alpha [b_{n+1,m}^* + b_{n-1,m}^* + b_{n,m+1}^* + b_{n,m-1}^* + 4b_{n,m}^*] = -\ddot{b}_{n,m} + 2i\omega_{\pi,\pi} \dot{b}_{n,m} + \omega_{\pi,\pi}^2 b_{n,m} \quad (24)$$

where $\alpha = 3a^2$. Looking for solutions of the form

$$b_{n,m} = A e^{i(Q_x n + Q_y m - \Omega t)} + B e^{-i(Q_x n + Q_y m - \Omega t)}, \quad (25)$$

we arrive at the following set of linear algebraic equations for the complex constants A and B

$$[(\Omega + \omega_{\pi,\pi})^2 - 8(1 + 2\alpha)\Delta] A + 8\alpha\Delta B = 0 \quad (26)$$

$$8\alpha\Delta A + [(\Omega - \omega_{\pi,\pi})^2 - 8(1 + 2\alpha)\Delta] B = 0, \quad (27)$$

where $2\Delta = \cos^2(Q_x/2) + \cos^2(Q_y/2)$. As for the one-dimensional case, we require that the determinant of this linear system in A and B vanishes, which leads to the following condition

$$[(\Omega + \omega_{\pi,\pi})^2 - 8\Delta(1 + 2\alpha)] [(\Omega - \omega_{\pi,\pi})^2 - 8\Delta(1 + 2\alpha)] = 64\alpha^2\Delta^2. \quad (28)$$

This equation admits two real and two complex conjugated imaginary solutions in Ω if

$$\Delta > \frac{1 + \alpha}{1 + 3\alpha}, \quad (29)$$

which is the analogous of condition (9) for two dimensions. One can achieve the minimal nonzero value of the r.h.s. of the above expression choosing $Q_x = 0$, $Q_y = 2\pi/N$, which leads to the following result for the critical amplitude

$$a_c = \left(\frac{\sin^2(\pi/N)}{3[3\cos^2(\pi/N) + 1]} \right)^{1/2}. \quad (30)$$

Its large N limit is

$$a_c = \frac{\pi}{\sqrt{12}N} + O\left(\frac{1}{N^3}\right). \quad (31)$$

This prediction is compared with numerical data in Fig. 1. The agreement is good for all values of N .

Since the relation between energy and amplitude is now $E = 2N^2(2a^2 + 4a^4)$, we obtain the critical energy in the large N -limit as

$$E_c = \frac{\pi^2}{3} + O\left(\frac{1}{N^2}\right). \quad (32)$$

This shows that the critical energy is now constant in the thermodynamic limit, which agrees with the remark of Ref. [44] about the existence of a minimal energy for breathers formation [23].

The results of this Section can be easily extended to any dimension d . Repeating the same argument, we arrive at the following estimates for the critical amplitude and energy in the large N limit

$$a_c = \frac{\pi}{\sqrt{6d}} \frac{1}{N} + O\left(\frac{1}{N^3}\right) \quad (33)$$

$$E_c = \frac{\pi^2}{3} N^{d-2} + O(N^{d-4}). \quad (34)$$

This means that the critical energy density $\varepsilon_c = E_c/N$ for destabilizing the zone boundary mode vanishes as $1/N^2$, independently of dimension.

2.3 Large N limit using the Nonlinear Schrödinger equation

The large N limit expressions (33) and (34) can be derived also by continuum limit considerations. We will derive the general expression for any dimension d . The displacement field can be factorized into a complex envelope part ψ multiplied by the zone boundary mode pattern in d dimensions.

$$u_{n_1, \dots, n_d} = \frac{\psi(n_1, \dots, n_d, t)}{2} e^{i(\pi \sum_{i=1}^d n_i - \omega_{\pi, \dots, \pi} t)} + c.c., \quad (35)$$

where

$$\omega_{\pi, \dots, \pi} = \sqrt{d[4(1 + 3|\psi|^2)]}. \quad (36)$$

Substituting Eq. (35) into the FPU lattice equations in d dimensions, a standard procedure [51, 50] leads to the following d dimensional Nonlinear Schrödinger (NLS) equation:

$$i \frac{\partial \psi}{\partial t} + \frac{P}{2} \Delta_d \psi - Q \psi |\psi|^2 = 0, \quad (37)$$

where Δ_d is the d dimensional Laplacian. The parameters P and Q are derived from the nonlinear dispersion relation

$$\omega^2 = \sum_{i=1}^d \left[4 \sin^2 \frac{q_i}{2} + 12 |\psi|^2 \sin^4 \frac{q_i}{2} \right], \quad (38)$$

as

$$P = \frac{\partial^2 \omega}{\partial q_i^2} (q_1 = \pi, \dots, q_d = \pi, |\psi| = 0) = \frac{1}{2\sqrt{d}} \quad (39)$$

$$Q = -\frac{\partial \omega}{\partial |\psi|^2} (q_1 = \pi, \dots, q_d = \pi, |\psi| = 0) = -3\sqrt{d}. \quad (40)$$

Assuming that, at the first stage, modulation instability develops along a single direction x and that the field remains constant along all other directions, one gets the one-dimensional NLS equation

$$i \frac{\partial \psi}{\partial t} + \frac{P}{2} \frac{\partial^2 \psi}{\partial x^2} - Q \psi |\psi|^2 = 0. \quad (41)$$

Following the results of the inverse scattering approach [17], any initial distribution of amplitude $|\psi|$ and length λ along x , and constant along all other directions, produces a final localized distribution if [18]

$$(|\psi| \lambda)^2 > \pi^2 \left| \frac{P}{Q} \right|. \quad (42)$$

This means that if the initial state is taken with constant amplitude $|\psi| = a$ on the d -dimensional lattice with N^d oscillators, the modulation instability threshold is

$$(a_c N)^2 = \frac{\pi^2}{6d} \quad (43)$$

which coincides with the leading order in Eq. (33).

3 Emergence of Localizations in Anti-FPU

3.1 Conservative Case: Chaotic Breathers

In this Section, we will discuss what happens when the modulational energy threshold is overcome. The first thorough study of this problem can be found in Ref. [21], many years after the early pioneering work of Zabusky and Deem [4]. Already in Ref. [21], it has been remarked that an energy localization process takes place, which leads to the formation of breathers [23]. This process has been further characterized in terms of time-scales to reach energy equipartition and quantitative localization properties in Ref. [24]. The localized structure which emerges after modulational instability has been here called ‘‘chaotic breather’’ (CB). The connection between CB formation and continuum equations has been discussed in Refs. [25, 27], while the relation with the process of relaxation to energy equipartition has been further studied in Ref. [26]. We will briefly recall some features of the localization process in one dimension and present new results for two dimensions.

For long time simulations, we use appropriate symplectic integration schemes in order to preserve as far as possible the Hamiltonian structure. For the one dimensional FPU, we adopt a 6th-order Yoshida’s algorithm [52] with a time step $dt = 0.01$; this choice allows us to obtain an energy conservation with a relative accuracy $\Delta E/E$ ranging from 10^{-10} to 10^{-12} . For two dimensions, we use instead the 5-th order symplectic Runge–Kutta–Nyström algorithm of Ref. [53], which gives a similar quality of energy conservation.

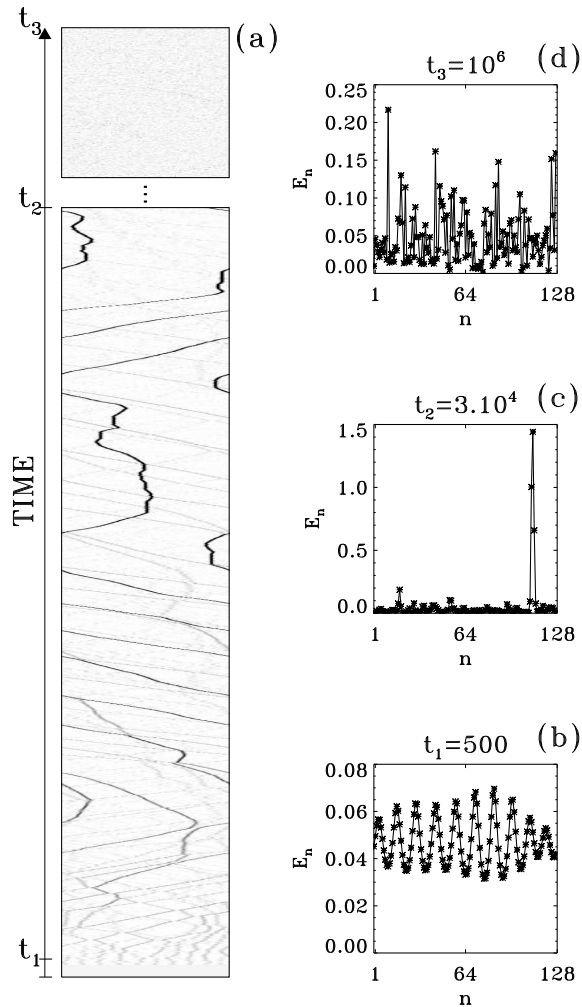


Fig. 2. Time evolution of the local energy (44). In panel (a), the horizontal axis indicates lattice sites and the vertical axis is time. The grey scale goes from $E_n = 0$ (white) to the maximum E_n -value (black). The lower rectangle corresponds to $0 < t < 3000$ and the upper one to $5.994 \cdot 10^5 < t < 6.10^5$. Figs. (b), (c) and (d) show the instantaneous local energy E_n along the $N = 128$ chain at three different times. Remark the difference in vertical amplitude in panel (c), when the CB is present. The initial π -mode amplitude is $a = 0.126 > a_c \simeq 0.010$.

We report in Fig. 2(a) a generic evolution of the one dimensional π -mode above the modulation instability critical amplitude ($a > a_c$). The grey scale refers to the energy residing on site n ,

$$E_n = \frac{1}{2}\dot{u}_n^2 + \frac{1}{2}V(u_{n+1} - u_n) + \frac{1}{2}V(u_n - u_{n-1}), \quad (44)$$

where the FPU-potential is $V(x) = \frac{1}{2}x^2 + \frac{1}{4}x^4$. Figs. 2(b), 2(c) and 2(d) are three successive snapshots of the local energy E_n along the chain. At short time, a slight modulation of the energy in the system appears (see Fig. 2(b)) and the π -mode is destabilized [13]. Later on, as shown in Fig. 2(a), only a few localized energy packets emerge: they are breathers [23]. Inelastic collisions of breathers have a systematic tendency to favour the growth of the big breathers at the expense of small ones [54,55]. Hence, in the course of time, the breather number decreases and only one, of very large amplitude, survives (see Fig. 2(c)): this is the localized excitation we have called chaotic breather (CB). The CB moves along the lattice with an almost ballistic motion: sometimes it stops or reflects. During its motion the CB collects

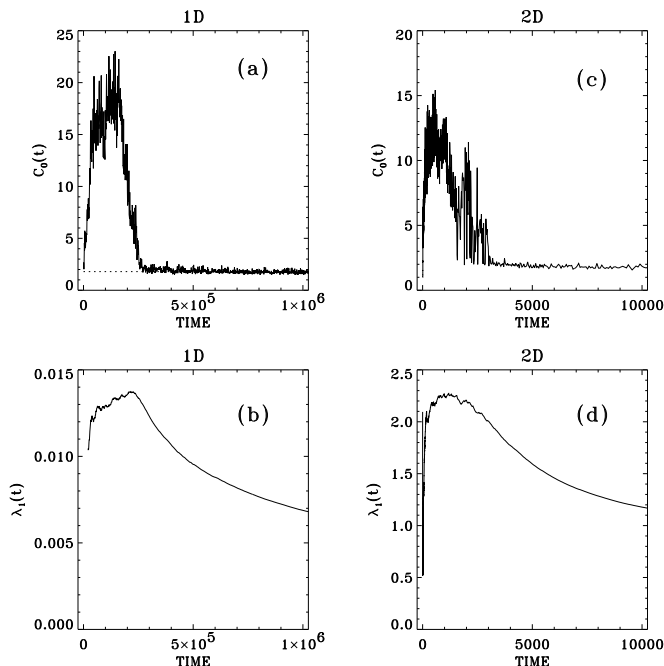


Fig. 3. Panel (a) presents the evolution of $C_0(t)$ of formula (45) for the one-dimensional FPU lattice with $N = 128$ oscillators, initialized on the π -mode with an amplitude $a = 0.126 > a_c \simeq 0.010$. The dashed line indicates the equilibrium value $\bar{C}_0 = 1.795$. Panel (b) presents the corresponding finite time largest Lyapunov exponent. Panel (c) shows $C_0(t)$ for the two-dimensional FPU lattice with $20 * 20$ oscillators, initialized on the (π, π) -mode with an amplitude $a = 0.425 > a_c \simeq 0.045$. Panel (d) presents the finite time largest Lyapunov exponent for two dimensions.

energy and its amplitude increases. It is important to note that the CB is never at rest and that it propagates with a given subsonic speed [56]. Finally, the CB decays and the system reaches energy equipartition, as illustrated in Fig. 2(d).

In order to obtain a quantitative characterization of energy localization, we introduce the “participation ratio”

$$C_0(t) = N \frac{\sum_{i=1}^N E_i^2}{\left(\sum_{i=1}^N E_i\right)^2}, \quad (45)$$

which is of order one if $E_i = E/N$ at each site of the chain and of order N if the energy is localized on only one site. In Fig. 3(a), C_0 is reported as a function of time. Initially, C_0 grows, indicating that the energy, evenly distributed on the lattice at $t = 0$, localizes over a few sites. This localized state survives for some time. At later times, C_0 starts to decrease and finally reaches an asymptotic value \bar{C}_0 which is associated with the disappearance of the CB (an estimate of \bar{C}_0 has been derived in Ref. [24] taking into account energy fluctuations and is reported with a dashed line in Fig. 3(a)). At this stage, the energy distribution in Fourier space is flat, i.e. a state of energy equipartition is reached.

In Fig. 3(b), we show the finite time largest Lyapunov exponent $\lambda_1(t)$ for the same orbit as in Fig. 3(a). We observe a growth of $\lambda_1(t)$ when the CB emerges on the lattice and a decrease when it begins to dissolve. The peak in $\lambda_1(t)$ perfectly coincides with the one in C_0 . Due to this increase of chaos associated with localization, we have called the breather chaotic (although chaos increase could be the result of more complicated processes of interaction with the background).

In Ref. [24], the time-scale for the relaxation to equipartition has been found to increase as $(E/N)^{-2}$ in the small energy limit. This has been confirmed by the followers of this study [25–27]. Such power law scalings are found also for the FPU relaxation starting from long wavelengths [57]: the so-called *FPU problem*. We have termed the relaxation process which starts from short wavelengths the *Anti-FPU problem*, just because of the similarities in the scaling laws. The main feature of the latter problem is that relaxation to equipartition goes through a complex process of localized structures formation well described by breathers or, in the low-amplitude limit, by solitons of the NonLinear Schrodinger equation. On the contrary, for the original FPU problem, an initial long wavelength excitation breaks up into a train of mKdV-solitons. The final relaxation to equipartition is however due to an energy diffusion process which has similar features for both the FPU and the anti-FPU problem [26].

A similar evolution of the local energy

$$E_{n,m} = \frac{1}{2}\dot{u}_{n,m}^2 + \frac{1}{4}V(u_{n+1,m} - u_{n,m}) + \frac{1}{4}V(u_{n,m+1} - u_{n,m}) + \frac{1}{4}V(u_{n-1,m} - u_{n,m}) + \frac{1}{4}V(u_{n,m-1} - u_{n,m}) \quad (46)$$

is observed for the two-dimensional case (see Fig. 4). In this figure, we just show the initial evolution which leads to the breathers formation. As for the one-dimensional case, bigger breathers eat up smaller ones, and finally only two breathers survive. We don't observe coalescence to a single breather because collisions are more rare in two dimensions. After the formation of a few localized structures, one also observes the final relaxation to equipartition which is not shown in Fig. 4. This latter is instead evident from the time evolution of $C_0(t)$, the localization parameter, shown in Fig. 3(c): its behavior is very similar to the one-dimensional case. Indeed, also the largest finite time Lyapunov exponent behaves similarly (see Fig. 3(d)).

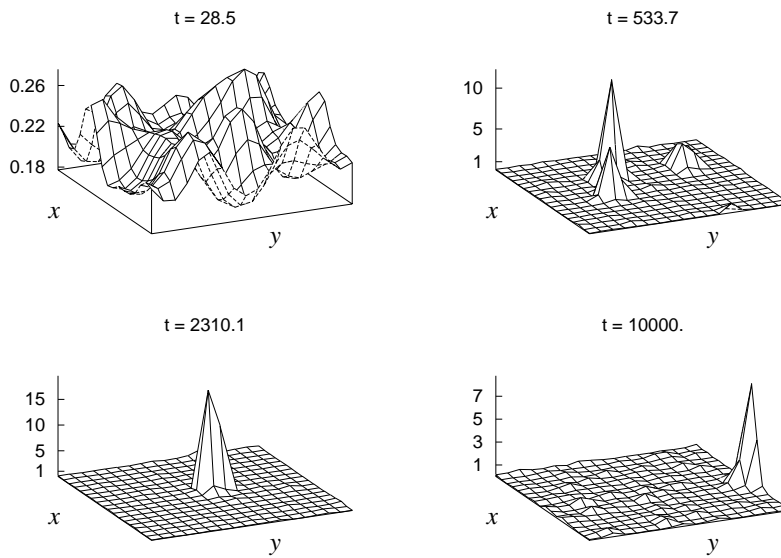


Fig. 4. Local energy (46) surface plots for the two-dimensional FPU lattice with $20 * 20$ oscillators, initialized on the (π, π) -mode with an amplitude $a = 0.225496 > a_c \simeq 0.0453450$. Snapshots at four different times t are shown. Breathers form after a coalescence process similarly to the one-dimensional case. The mobility of the breathers is evident and one also observes in the last panel the final decrease.

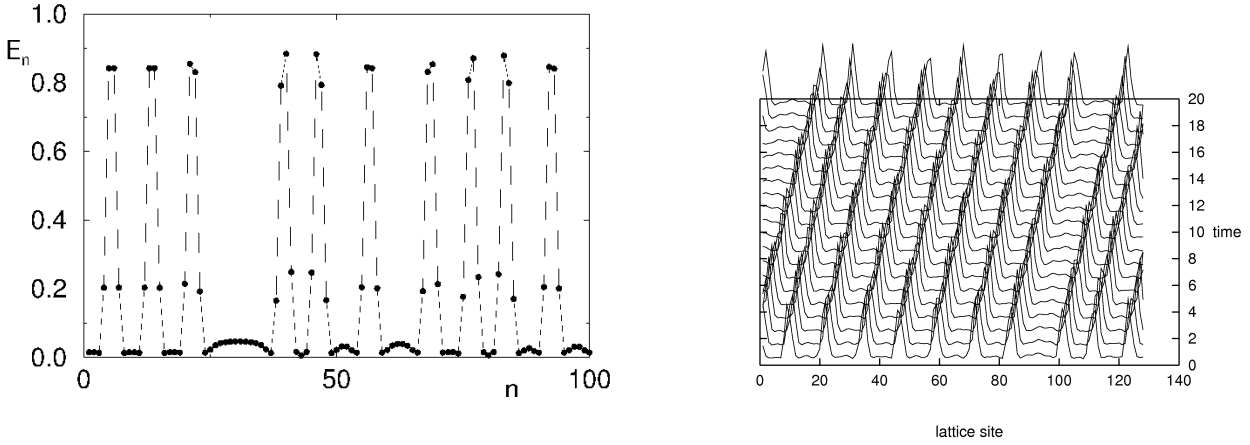


Fig. 5. Left panel: Static multibreather pattern generated after the modulational instability for $p = \pi$ ($\omega = 2.4$, $f = 0.2250$). This pattern stabilizes at $t \simeq 5 \cdot 10^3$. Right panel: Travelling multibreather pattern of the $p \neq \pi$ -mode for a lattice of $N = 512$ sites. Here, $\omega = 2.05$, $f = 0.075$ and $p = 2.4542$.

3.2 Nonconservative Case: Homogeneously Driven-Damped Anti-FPU

The equations of motion of the “externally driven” and damped FPU chain read as follows:

$$\ddot{u}_n = u_{n+1} + u_{n-1} - 2u_n + (u_{n+1} - u_n)^3 + (u_{n-1} - u_n)^3 - \gamma \dot{u}_n + f \cos(\omega t + pn), \quad (47)$$

where the forcing and damping strengths are gauged by the parameters f and γ , respectively; ω and p are the driving frequency and wavenumber. Considering the Anti-FPU situation, we restrict ourselves to the case $\pi/2 < |p| < \pi$. Moreover, here we present only the results concerning the range of driving frequencies $|\omega| > \omega_p \equiv \sqrt{2(1 - \cos p)}$ for which stationary multibreather states develop (they are static if $p = \pi$ and move for other cases). For other driving frequencies, one deals with the stationary periodic patterns described in Refs. [64,65].

Examples of appearance of either static ($p = \pi$) or traveling ($p \neq \pi$) multibreather states are shown in Fig. 5, where we plot the local energy vs. the lattice position sampled at the period of the forcing. The corresponding spatial Fourier spectrum is shown in Fig. 6. The broad band structure of the spectrum reflects the non perfect periodic arrangement of the localized peaks in Fig. 5.

Such states can be described in terms of soliton solutions of an associated suitable driven-damped nonlinear Schrödinger (NLS) equation. Let us first make the following definition:

$$u_n = \frac{1}{2} \left[a_p(n, t) e^{i(\omega t + pn)} + a_p^+(n, t) e^{-i(\omega t + pn)} \right], \quad (48)$$

where a_p and its conjugate are smooth functions of n . Such an assumption is possible if the wavepacket is concentrated around the driving mode $\Delta k \ll \pi$. Substituting (48) into the equations of motion (47), one gets:

$$(\omega_p^2 - \omega^2) a_p + 2i\omega \left(\frac{\partial a_p}{\partial t} - v \frac{\partial a_p}{\partial n} \right) + \frac{\omega_p^2}{4} \frac{\partial^2 a_p}{\partial n^2} + \frac{3}{4} \omega_p^4 a_p |a_p|^2 = -i\omega \gamma a_p - f. \quad (49)$$

After performing the following re-scalings

$$t' = \frac{\omega^2 - \omega_p^2}{2\omega} t, \quad \xi = \frac{2\sqrt{\omega^2 - \omega_p^2}}{\omega_p} (n - vt),$$

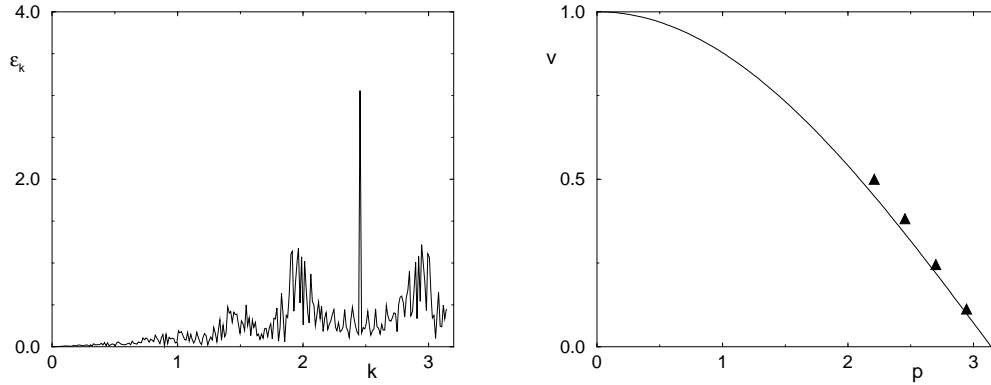


Fig. 6. Left panel: Spatial spectrum of the travelling multibreather. $\epsilon_k = |\dot{U}_k| + \omega^2|U_k|$, where U_k is the k -th component of the Fourier spectrum of the displacement field u_n . Same parameters as in Fig. 5. Right panel: Velocity (triangles) of travelling multibreathers versus the wavenumber of the forcing. The solid line is the group velocity of linear waves.

$$\Psi = \sqrt{\frac{3}{8}} \frac{\omega_p^2}{\sqrt{\omega^2 - \omega_p^2}} e^{it'} a_p(\xi, t'), \quad \gamma' = \frac{\omega}{\omega^2 - \omega_p^2} \gamma, \quad h = \sqrt{\frac{3}{8}} \frac{\omega_p^2}{(\omega^2 - \omega_p^2)^{3/2}} f,$$

and choosing a reference frame moving with velocity $v = \partial\omega_p/\partial p = \sin p/\omega_p$, Eq. (49) reduces to the well studied “externally” driven (or ac driven) damped NLS equation [66,67]:

$$i \frac{\partial \Psi}{\partial t'} + \frac{\partial^2 \Psi}{\partial \xi^2} + 2\Psi|\Psi|^2 = -i\gamma'\Psi - h e^{it'}. \quad (50)$$

Exact soliton solutions of this equation can be obtained for $\gamma' = 0$, see Eqs. (37-40) of Ref. [66]. Moreover, multisoliton solutions are also derived in Ref. [67]. What we observe in Fig. 5 might well be a superposition of such solutions to form a train of “intrinsically localized” structures. However, one should bear in mind that NLS solutions can describe only low amplitude states. Therefore, they can be only a rough approximation of the pattern displayed in Fig. 5, which shows high amplitude localized peaks.

In the right panel of Fig. 6, we plot the speed of the travelling multibreather as a function of the wavenumber of the forcing p -mode, which compares well with the group velocity of the corresponding linear waves, showing that nonlinear effects are negligible in this parameter range.

3.3 Driving by one end: Ordinary and Bandgap Transmission

To simulate the effect of an impinging wave, we impose to the β -FPU chain [$\ell = 1$ in Eq. (1)], the boundary condition

$$u_0(t) = A \cos \omega t, \quad (51)$$

while free boundary conditions are enforced on the other side of the chain.

In order to be able to observe a stationary state in the *conducting* regime, we need to steadily remove the energy injected in the lattice by the driving force. Thus, we damp a certain number of the rightmost sites (typically 10% of the total) by adding a viscous term $-\gamma \dot{u}_n$ to their equations of motion. A convenient indicator to look at is the averaged energy flux $j = \sum_n j_n/N$, where the local flux j_n is given by the following formula [68]

$$j_n = \frac{1}{2} (\dot{u}_n + \dot{u}_{n+1}) [u_{n+1} - u_n + (u_{n+1} - u_n)^3]. \quad (52)$$

Time averages of this quantity are taken in order to characterize the insulating (zero flux)/conducting (non zero flux) state of the system.

3.3.1 In-band driving: nonlinear phonons

For illustration, we first discuss the case when the driving frequency is located inside the phonon band. Although trivial, this issue is of importance to better appreciate the fully nonlinear features described later on.

Under the effect of the driving (51), we can look for extended quasi-harmonic solutions (nonlinear phonons) of the form

$$u_n = A \cos(kn - \omega t). \quad (53)$$

We consider the semi-infinite chain, so that k varies continuously between 0 and 2π . The nonlinear dispersion relation can be found in the rotating wave approximation (see e.g. Ref. [69]). Neglecting higher-order harmonics, it reads

$$\omega_0^2(k, A) = 2(1 - \cos k) + 3(1 - \cos k)^2 A^2. \quad (54)$$

Thus the nonlinear phonon frequencies range from 0 to the upper band-edge $\omega_0(\pi, A) \geq 2$.

If we simply assume that only the resonating phonons whose wavenumbers satisfy the condition

$$\omega = \omega_0(k, A) \quad (55)$$

are excited, we can easily estimate the energy flux. Neglecting, for simplicity, the nonlinear force terms in the definition of the flux (52), we have

$$j = \frac{1}{2} v(k, A) \omega^2 A^2, \quad (56)$$

where v is the group velocity as derived from dispersion relation (54). This simple result is in very good agreement with simulations, at least for small enough amplitudes (see left panel of Fig. 7). For $A > 0.15$, the measured flux is larger than the estimate (56), indicating that something more complicated occurs in the bulk (possibly, a multiphonon transmission) and that higher-order nonlinear terms must be taken into account.

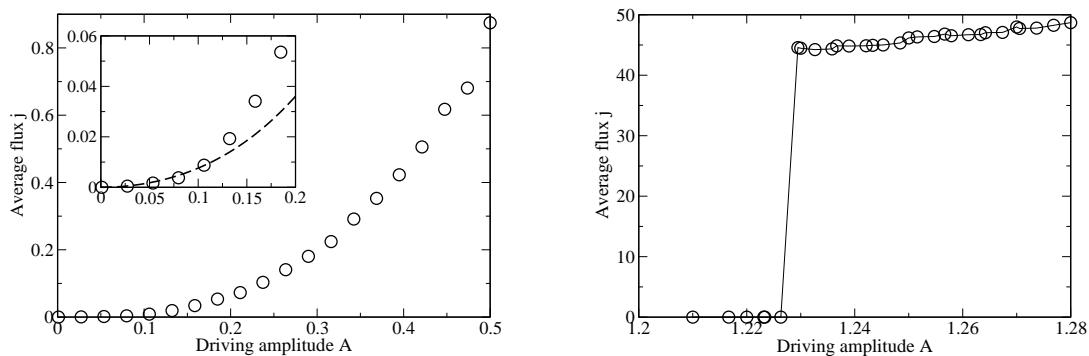


Fig. 7. Left panel: Average energy flux vs. driving amplitude for in-band forcing, $\omega = 1.8$, $\gamma = 5$. Data have been averaged over 10^5 periods of the driving. The inset is an enlargement of the small-amplitude region and the dashed line is the single nonlinear phonon approximation (56). Right panel: Average energy flux vs. driving amplitude for out-band forcing, $\omega = 3.5$, $\gamma = 5$. Data have been averaged over $2 \cdot 10^5$ periods of the driving for a chain of $N = 512$ particles.

3.3.2 Out-band driving: supratransmission

Let us now turn to the more interesting case in which the driving frequency lies outside the phonon band, $\omega > \omega_0(\pi, 0) = 2$. In a first series of numerical experiments, we have initialized the chain at rest and switched on the driving at time $t = 0$. To avoid the formation of sudden shocks [70], we have chosen to increase smoothly the amplitude from 0 to the constant value A at a constant rate, i.e.

$$u_0 = A \cos(\omega t) \left[1 - e^{-t/\tau_1} \right], \quad (57)$$

where typically we set $\tau_1 = 10$.

At variance with the case of in-band forcing, we observe a sharp increase of the flux at a given threshold amplitude of the driving, see right panel of Fig. 7. This phenomenon has been denoted as *nonlinear supratransmission* [38] to emphasize the role played by nonlinear localized excitations in triggering the energy flux.

This situation should be compared with the one of in-band driving, shown in Fig. 7, where no threshold for conduction exists and the flux increases continuously from zero (more or less quadratically in the amplitude). Indeed, the main conclusion that can be drawn from the previous section is that there cannot be any amplitude threshold for energy transmission in the case of in-band forcing. Moreover, although at the upper band edge the flux vanishes, since it is proportional to the group velocity (see formula (56)), it is straightforward to prove that it goes to zero with the square root of the distance to the band edge frequency. Hence, the sudden jump we observe in the out-band case cannot be explained by any sort of quasi-linear approximation.

In the following, we investigate the physical origin of nonlinear supratransmission, distinguishing the cases of small and large amplitudes.

When the driving frequency is only slightly above the band ($0 < \omega - 2 \ll 1$), one can resort to the continuum envelope approximation. Since we expect the zone-boundary mode $k = \pi$ to play a major role, we let

$$u_n = (-1)^n \frac{1}{2} [\psi_n e^{i\omega t} + \psi_n^* e^{-i\omega t}]. \quad (58)$$

In the rotating wave approximation [69] and for slowly varying ψ_n , one obtains from the FPU lattice equations the nonlinear Schrödinger equation ($\psi_n \rightarrow \psi(x, t)$) [71]

$$2i\omega\dot{\psi} = (\omega^2 - 4)\psi - \psi_{xx} - 12\psi|\psi|^2, \quad (59)$$

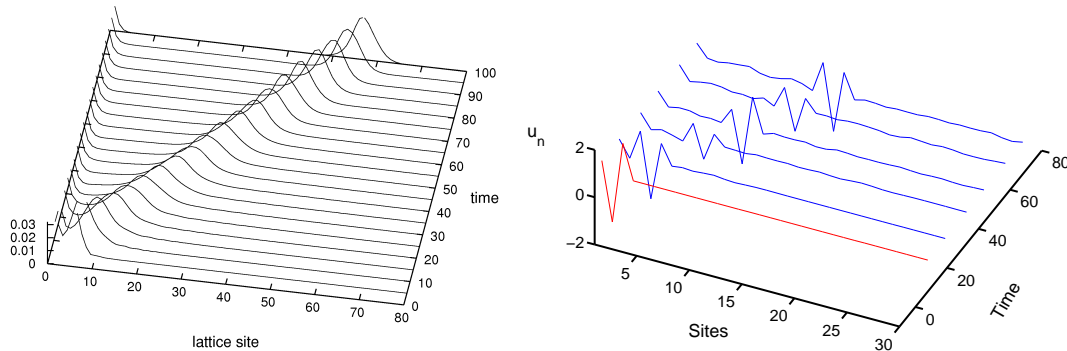


Fig. 8. Left panel: Snapshot of the local energy below the supratransmission threshold $A = 0.15 < A_{th}$ for $\omega = 2.1$ $\gamma = 10$. The initial condition is an envelope soliton (60) with $x_0 = +1.8$. Right panel: Snapshot of particle displacements u_n below the supratransmission threshold for a driving frequency $\omega = 5.12$ and a driving amplitude $A = 0.5 < A_{th} = 2.05$. One can observe, similarly to the left panel, that a moving discrete breather appears at the left boundary and propagates inside the bulk, leaving behind the static solution.

with the boundary condition $\psi(0, t) = A$.

The well-known *static* single-soliton solution of Eq. (59) corresponds to the family of envelope solitons (low-amplitude discrete breathers)

$$u_n = a(-1)^n \cos(\omega t) \operatorname{sech} \left[\sqrt{6}(n - x_0)a \right], \quad (60)$$

with amplitude $a = \sqrt{(\omega^2 - 4)/6}$. The maximum of the soliton shape is fixed by the boundary condition to be

$$x_0 = \pm \frac{\operatorname{acosh}(a/A)}{a\sqrt{6}}. \quad (61)$$

In this approximation, we have two possible solutions: one with the maximum outside the chain, which is purely decaying inside the chain (minus sign in (61)), and another with the maximum located within the chain (plus sign in (61)). Overcoming the supratransmission threshold corresponds to the disappearance of both solutions. Indeed, when the driving amplitude reaches the critical value A_{th} , given by

$$\omega^2 = 4 + 6A_{th}^2, \quad (62)$$

solution (60) ceases to exist.

We have investigated this issue by simulating the lattice dynamics with the initial conditions given by Eqs. (60) and (61). The evolution of the local energy E_n (see Eq. (44)) is shown in left panel of Fig. 8. The solution with the maximum inside the chain slowly moves towards the right and, eventually, leaves a localized boundary soliton (with maximum outside the chain) behind. The release of energy to the chain is non stationary and does not lead to a conducting state.

The scenario drastically changes at the supratransmission amplitude A_{th} . The chain starts to conduct: a train of *travelling* envelope solitons is emitted from the left boundary (see left panel of Fig. 9). Here we should emphasize that the envelope soliton solution (60), which is characterized by the $k = \pi$ carrier wave-number, has a zero group velocity. Thus, transmission cannot be realized by such envelope solitons. Instead, transmission starts when the driving frequency resonates with the frequency of the envelope soliton with carrier wave-number $k = \pi(N - 2)/N$, next to the π -mode. However, as far as we consider a large number of oscillators ($N = 500$), we can still use expression (62) for the π -mode frequency.

The above envelope soliton solution (60) is valid in the continuum envelope limit, and is therefore less and less accurate as its amplitude increases. Indeed, if the weakly nonlinear condition is violated, the width of the envelope soliton becomes comparable with lattice spacing and, thus, one cannot use the continuum envelope approach. Fortunately, besides the slowly varying envelope soliton solution (60), an analytic approximate expression exists for large amplitude static discrete breather solutions, which is obtained from an exact extended plane wave solution with “magic” wave-number $2\pi/3$ [72]

$$u_n = a(-1)^n \cos[\omega_B(a)t] \cos\left(\frac{\pi}{3}n \pm x_0\right), \quad (63)$$

if $|(\pi n/3) \pm x_0| < \pi/2$ and $u_n = 0$ otherwise.

Here x_0 is defined as follows

$$x_0 = \operatorname{acos}(A/a), \quad (64)$$

where A is the driving amplitude. The breather frequency $\omega_B(a)$ depends on amplitude a as follows

$$\omega_B(a) \simeq 1.03 \frac{\sqrt{3\pi^2(4 + 9a^2)}}{4K(s)}, \quad (65)$$

where $K(s)$ is the complete elliptic integral of the first kind with argument $s = 3a/\sqrt{2(9a^2 + 4)}$ and the factor 1.03 takes into account a rescaling of the frequency of the “tailed” breather [73] (see also [74]). As previously for the case of the envelope soliton solution, we perform a numerical experiment where we put initially on the lattice the breather solution of formula (63). Choosing

the plus sign in this expression, we do not observe any significant transmission of energy inside the chain. Instead, the minus sign causes the appearance of a moving breather, which travels inside the chain leaving behind the static breather solution with plus sign. Right graph in Fig. 8 presents this numerical experiment.

The static breather solution (63) ceases to exist if the driving amplitude exceeds the threshold A_{th} given by the resonance condition

$$\omega = \omega_B(A_{th}). \quad (66)$$

Above this threshold the supratransmission process begins via the emission of a train of moving breathers from the boundary, exactly as it happens in the case of small amplitudes. It should be mentioned again that the transmission regime is established due to moving discrete breathers. It has been remarked [72] that discrete breathers are characterized by quantized velocities, while their frequency is given by the same formula (65). This explains why one can use resonance condition (66) for the static discrete breather solution (63) to define the supratransmission threshold in the large amplitude limit.

3.3.3 Supratransmission threshold: numerical test

To check these predictions, we have performed a numerical determination of A_{th} for several values of ω , starting the chain at rest. This is accomplished by gradually increasing A and looking for the minimal value A_{th} for which a sizeable energy propagates into the bulk of the chain. At early time, the scenario is qualitatively similar to the one shown in the left graph of Fig. 9. Later on, the interaction of nonlinear and quasi-linear modes and their “scattering” with the dissipating right boundary establishes a steady energy flux into the chain.

As seen in the right graph of Fig. 9, formulae (66) [with definition (65)] and (62) (see the inset) are in excellent agreement with simulations for large $A > 2$ and small $A \leq 1$ amplitudes, respectively. The accuracy of the analytical estimate in formulae (66) and (62) is of the order of few percents, at worst, in the intermediate amplitude range.

For comparison, we have checked that the supratransmission threshold is definitely not associated with the quasi-harmonic waves with nonlinear dispersion relation (54). If this were

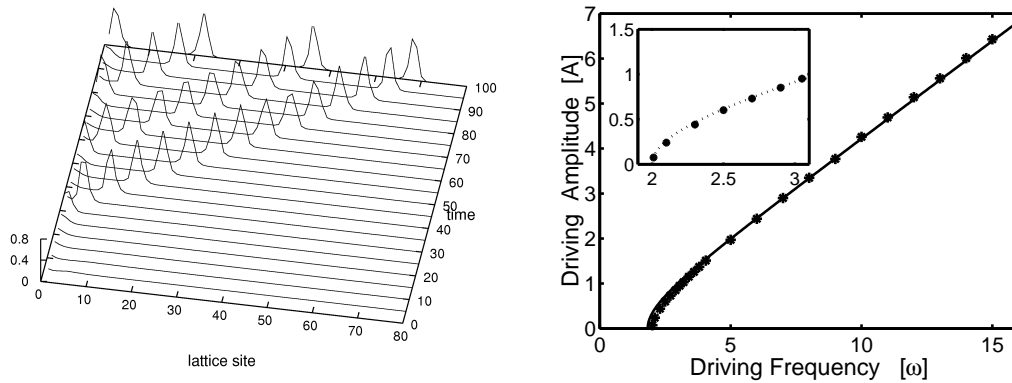


Fig. 9. Left graph: Snapshot of the local energy at the transmission threshold $A = 0.253 \approx A_{th}$ for $\omega = 2.1$ $\gamma = 10$. The initial condition is the envelope soliton (60) with $x_0 \approx 0$. Right graph: Comparison between analytic estimates and numerical values of threshold amplitudes vs. the driving frequency. Main plot: the full dots are the numerical values of A_{th} and the solid line is a plot of formulae (65-66), which are valid for large amplitudes. The inset shows an enlargement of the small A_{th} region, in order to illustrate the accuracy of the small-amplitude approximation (62) (dotted line).

the case, the transmission should start when the oscillation amplitude reaches the value for which the resonance condition $\omega = \omega_0(k, A)$ holds. As $\omega_0(k, A)$ is maximal for $k = \pi$, we can get the expression for the threshold value from the relation $\omega = \omega_0(\pi, A_{th})$, i.e.

$$\omega^2 = 4 + 12A_{th}^2. \quad (67)$$

The amplitude values one obtains from Eq. (67) are far away from the numerical values and we don't even show them in the right graph of Fig. 9. This is a further confirmation that supratransmission in the FPU model originates from direct discrete breather generation as it happens in the cases of discrete sine-Gordon and nonlinear Klein-Gordon lattices [38].

4 Conclusions

In this paper, we have presented a detailed analysis of the zone-boundary mode modulational instability for the FPU lattice in both one and higher dimensions. Formulas for the critical amplitude have been derived analytically and compare very well with numerics for all system sizes. The study of the process which leads to the formation of chaotic breathers can be extended to two dimension; the physical picture is similar to the one-dimensional case.

All results on modulational instability of zone-boundary modes can be straightforwardly extended to other initial modes and, correspondingly, instability rates can be derived. This has already been partially done in Ref. [14] and compares very well with the numerical results by Yoshimura [58]. This author has recently reanalyzed the problem [59] to determine the growth rates for generic nonlinearities in the high energy region, obtaining exact results based on Mathieu's equation.

For many-modes initial excitations, it has been remarked that instability thresholds depend on relative amplitudes and not only on the total energy [9]. Although this makes the study of the problem extremely involved, we believe that a detailed study of some selected group of modes, which play some special role in FPU dynamics, could be interesting. The method discussed in this paper could be adapted to treat this problem. Historically, the first study is in the paper by Bivins, Metropolis and Pasta himself [60], where the authors tackle the problem by studying numerically the instabilities of coupled Mathieu's equations.

In one-dimensional studies, a connection between the average modulation instability rates and the Lyapunov exponents has been suggested [11, 14]. Recently [62], high frequency exact solutions have been used in the context of a differential geometric approach [63] to obtain accurate estimates of the largest Lyapunov exponent. Similar studies could be performed for the two-dimensional FPU lattice and the corresponding scaling laws with respect to energy density could be obtained.

Finally, let us point out the generic nature of the results derived for the driven-damped Anti-FPU scenario. In this connection further developments towards nonlinear supratransmission and bistability effects in various physical systems, such as magnetic thin films [75], Josephson junction arrays [76], quantum Hall bilayers [77], optical directional couplers [78] and waveguide arrays [79, 80] should be especially mentioned.

Acknowledgement: We express our gratitude to all our collaborators in this field: J. Barré, M. Clément, T. Cretegnny, J. Leon, S. Lepri, P. Poggi, A. Torcini. We also thank N. J. Zabusky for useful exchanges of informations. This work is part of the PRIN contract *Dynamics and thermodynamics of systems with long-range interactions*. R.Kh. is supported by the Marie-Curie incoming fellowship award (MIF2-CT-2006-021328) and USA CRDF Award # GEP2-2848-TB-06.

References

1. E. Fermi, J. Pasta, S. Ulam, Los Alamos Science Laboratory Report No. LA-1940 (1955), unpublished; reprinted in *Collected Papers of Enrico Fermi*, edited by E. Segré (University of Chicago

- Press, Chicago, 1965), Vol. 2, p 978. also in *Nonlinear Wave Motion*, Newell A. C. Ed., Lecture in Applied Mathematics **15** (AMS, Providence, Rhode Island, 1974) and in *The Many-Body Problem*, Mattis C. C. Ed. (World Scientific, Singapore, 1993).
2. J. Ford, Phys. Rep. **213**, 271 (1992).
 3. A. J. Lichtenberg, M. A. Lieberman, *Regular and chaotic dynamics* (Springer, Berlin, 1992). Chapt. 6.5.
 4. N. J. Zabusky, G. S. Deem, J. Comp. Phys. **2**, 126 (1967).
 5. N. Budinsky, T. Bountis, Physica D **8**, 445 (1983).
 6. S. Flach, Physica D **91**, 223 (1996).
 7. P. Poggi, S. Ruffo, Physica D **103**, 251 (1997).
 8. G. M. Chechin, N. V. Novikova, A. A. Abramenko, Physica D **166**, 208 (2002).
 9. G. M. Chechin, D. S. Ryabov, K. G. Zhukov, Physica D **203**, 121 (2005).
 10. B. Rink, Physica D **175**, 31 (2003).
 11. T. Dauxois, S. Ruffo, A. Torcini, Phys. Rev. E **56**, R6229 (1997).
 12. V. M. Burlakov, S. A. Darmanyany, V. N. Pyrkov, Sov. Phys. JETP **81**, 496 (1995).
 13. K. W. Sandusky, J. B. Page, Phys. Rev. B **50**, 866 (1994).
 14. T. Dauxois, S. Ruffo, A. Torcini, Journal de Physique IV **8**, 147 (1998).
 15. Yu. S. Kivshar, M. Peyrard, Phys. Rev. A **46**, 3198 (1992).
 16. T. B Benjamin, J. E. Feir, J. Fluid Mech. **27**, 417 (1967).
 17. V.E. Zakharov, A.B. Shabat, Zhurnal Eksperimentalnoi I Teoreticheskoi Fiziki **64**, 1627 (1973).
 18. V.P. Lukomskii, Ukr. Fiz. Zh. **23**, 134 (1978).
 19. G. P. Berman, A. R. Kolovskii, Zh. Eksp. Teor. Fiz. **87**, 1938 (1984) [Sov. Phys. JETP **60**, 1116 (1984)].
 20. I. Daumont, T. Dauxois, M. Peyrard, Nonlinearity **10**, 617 (1997).
 21. V. M. Burlakov, S. A. Kiselev, V. I. Rupasov, Phys. Lett. A **147**, 130 (1990); V. M. Burlakov and S. Kiselev, Sov. Phys. JETP **72**, 854 (1991).
 22. A. J. Sievers, S. Takeno, Phys. Rev. Lett. **61**, 970 (1988).
 23. T. Dauxois, A. Litvak-Hinenzon, R. S. MacKay, A. Spanoudaki (Eds), *Energy Localisation and Transfer*, Advanced Series in Nonlinear Dynamics, World Scientific (2004).
 24. T. Cretegy, T. Dauxois, S. Ruffo, A. Torcini, Physica D **121**, 109-126 (1998).
 25. Y. A. Kosevich, S. Lepri, Phys. Rev. B **61**, 299 (2000).
 26. K. Ullmann, A. J. Lichtenberg, G. Corso, Phys. Rev. E **61**, 2471 (2000).
 27. V. V. Mirnov, A. J. Lichtenberg, H. Guclu, Physica D **157**, 251 (2001).
 28. N. J. Zabusky, Z. Sun, G. Peng, Chaos **16**, 013130 (2006).
 29. K. Ø. Rasmussen, T. Cretegy, P. G. Kevrekidis and N. Grønbech-Jensen, Phys. Rev. Lett. **84**, 3740 (2000).
 30. M. Johansson and K. Ø. Rasmussen, Phys. Rev. E **70**, 066610 (2004).
 31. M. Johansson, Physica D **216**, 62 (2006).
 32. B. Gershgorin, Y. V. Lvov, D. Cai, Phys. Rev. Lett. **95**, 264302 (2005).
 33. S. Flach, V. Ivanchenko, O. I. Kanakov, Phys. Rev. Lett. **95**, 064102 (2005).
 34. J. Tailleur J, Kurchan, to be published in Nature Physics (2007); also cond-mat/0611672.
 35. S. Tanase-Nicola, J. Kurchan, Journal of Statistical Physics **116** 1201-1245 (2004).
 36. T. Dauxois, R. Khomeriki, F. Piazza, S. Ruffo, Chaos **15**, 015110 (2005).
 37. V.M. Burlakov, Phys. Rev. Lett. **80**, 3988 (1998).
 38. F. Geniet, J. Leon, Phys. Rev. Lett. **89**, 134102 (2002).
 39. R. Khomeriki, S Lepri, S. Ruffo, Phys. Rev. E **70**, 066626 (2004).
 40. P. Maniadis, G. Kopidakis and S. Aubry, Physica D **216**, 121 (2006).
 41. A. Cafarella, M. Leo, R. A. Leo, Phys. Rev. E **69**, 046604 (2004).
 42. F. M. Izraïlev, B. V. Chirikov, Dokl. Akad. Nauk. SSSR **166**, 57 (1966) [Sov. Phys. Doklady **11**, 30 (1966)].
 43. M. Pettini, M. Landolfi, Phys. Rev. A **41**, 768 (1990).
 44. S. Flach, K. Kladko, R. S. MacKay, Phys. Rev. Lett. **78**, 1207 (1997).
 45. D. W. Jepsen, J. Math. Phys. **6**, 405 (1965).
 46. J. Barré, rapport de stage de Maîtrise, ENS Lyon, “Instabilités des solutions périodiques et formation de breathers chaotiques dans le modèle FPU” (1998).
 47. M. Clément, rapport de stage de License, ENS Lyon, “Différentes études du modèle Fermi-Pasta-Ulam” (1996).
 48. S. Shinohara, J. Phys. Soc. Japan **71**, 1802 (2002); Prog. Theor. Phys. Suppl. **150** 423 (2003).
 49. B. Rink, F. Verhulst, Physica A **285**, 467 (2000); B. Rink, Comm. Math. Phys. **218**, 665 (2001).

50. T. Dauxois, M. Peyrard, *Physics of Solitons*, Cambridge University Press (2006).
51. M. Remoissenet, Phys. Rev. B **33**, 2386 (1986).
52. H. Yoshida, Phys. Lett. A **150**, 262 (1990).
53. J. M. Sanz-Serna, M. P. Calvo, *Numerical Hamiltonian Problems*, (London: Chapman & Hall) (1994).
54. T. Dauxois, M. Peyrard, Phys. Rev. Lett. **70**, 3935 (1993).
55. O. Bang, M. Peyrard, Phys. Rev. E **53**, 4143 (1996).
56. Y. A. Kosevich, G. Corso, Physica D **170**, 1 (2002).
57. J. DeLuca, A. J. Lichtenberg, S. Ruffo, Phys. Rev. E **60**, 3781 (1999).
58. K. Yoshimura, Physica D **104**, 148 (1997).
59. K. Yoshimura, Phys. Rev. E **70**, 016611 (2004).
60. R. L. Bivins, N. Metropolis, J. R. Pasta, J. Comp. Phys. **12**, 62 (1972).
61. G. Benettin, Chaos **15**, 015108 (2005).
62. R. Franzosi, P. Poggi, M. Cerruti-Sola, Phys. Rev. E **71**, 036218 (2005)
63. M. Pettini, Phys. Rev. E **47**, 828 (1993); L. Casetti, C. Clementi, M. Pettini, Phys. Rev. E **54**, 5969 (1996).
64. R. Khomeriki, S. Lepri, S. Ruffo, Phys. Rev. E **64**, 056606 (2001).
65. R. Khomeriki, S. Lepri, S. Ruffo, Physica D **168-169C**, 152 (2002).
66. I.V. Barashenkov, Yu. S. Smirnov, Phys. Rev. E. **54** 5707 (1996).
67. I.V. Barashenkov, Yu. S. Smirnov, N.V. Alexeeva, Phys. Rev. E. **57** 2350 (1998).
68. S. Lepri, R. Livi, A. Politi, Phys. Rep. **377**, 1, (2003).
69. S. Takeno, K. Kisoda, A.J. Sievers, Prog. Theor. Phys. Suppl. **94**, 242 (1988).
70. Yu. A. Kosevich, R. Khomeriki, S. Ruffo, Europhys. Lett. **66**, 21 (2004).
71. A.J. Scott, *Nonlinear science*, Oxford University Press (1999), Chapter 3.3.
72. Yu. A. Kosevich, Phys. Rev. Lett. **71**, 2058 (1993); Phys. Rev. B **47**, 3138, (1993).
73. Notice that a simpler approximate expression for the breather frequency has been proposed in [72] in the form $\omega_B = \sqrt{3 + 81A^2/16}$. We have checked that this expression is also in good agreement with numerical data, but we prefer to use the more accurate form in formula (65).
74. Yu. A. Kosevich, G. Corso, Physica D **170**, 1, (2002).
75. R. Khomeriki, J. Leon, M. Manna, Phys. Rev. B **74**, 094414 (2006).
76. D. Chevriaux, R. Khomeriki, J.Leon, Phys. Rev. B **73**, 214516 (2006).
77. R. Khomeriki, D. Chevriaux, J.Leon, Eur. Phys. J. B **49**, 213 (2006).
78. D. Chevriaux, R. Khomeriki, J. Leon, Modern Phys. Lett. B **20**, 515 (2006).
79. R. Khomeriki, Phys. Rev. Lett. **92**, 063905, (2004).
80. R. Khomeriki, J. Leon, Phys. Rev. Lett. **94**, 243902 (2005).